CYBER
Pharmacodia AI

# CYBER AIDD

## WEEKLY REPORT

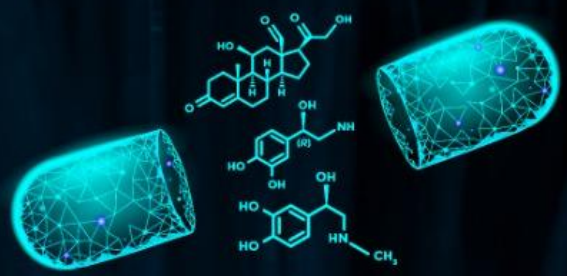


CyberAIDD assisted analysis of drug discovery article Titled **"Discovery and functional characterization of a potent, selective and metabolically stable PROTAC and Protein kinases DYRK1A and DYRK1B**
(Reference: **J. Med. Chem. 2024, 67, 19, 17259–17289)**

CyberAIDD assisted analysis of drug discovery article Titled **"Discovery and functional characterization of a potent, selective and metabolically stable PROTAC and Protein kinases DYRK1A and DYRK1B**

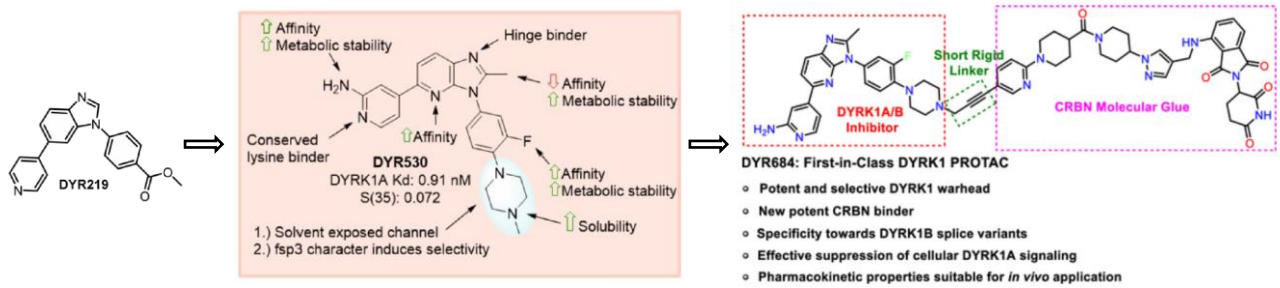


Small-molecule-induced targeted protein degradation is a promising approach for new drug discovery and development. Physiological and pathological processes such as neurodegeneration, tumorigenesis, and adaptive immunity are closely related to protein kinases DYRK1A and DYRK1B. A research team at the University of Arizona has developed a novel DYRK1 proteolysis-targeting chimera (PROTAC) for the first time by combining an ATP-competitive DYRK1 inhibitor with the E3 ligase ligand CRBN to induce ubiquitination and degradation of DYRK1A and DYRK1B. Among them, compound DYR684 can degrade DYRK1A rapidly, efficiently and selectively at the cellular level, while the splice variant of DYRK1B without enzymatic activity (p65) resists degradation. Compared with competitive kinase inhibition, the targeted degradation of DYRK1 by DYR684 better inhibited the downstream signal, indicating that DYRKs are a feasible target for PROTAC development, and DYR684 is expected to be a specific chemical probe for DYRK1A and DYRK1B.

The Pharmacodia CyberSAR System provides an in-depth analysis of DYRK1 inhibitor molecules. The system shows the active molecules associated with the target through the cluster structure view and the original structure view, and presents the potential Hit in the form of a timeline of the R&D stage. In addition, CyberSAR also provides visual analysis of indications and trial design, helping developers quickly obtain target structure information and develop research ideas. Although CyberSAR was not used in the initial development of the molecule in this case, it has shown great potential for application in the elucidation and optimization of drug molecules.

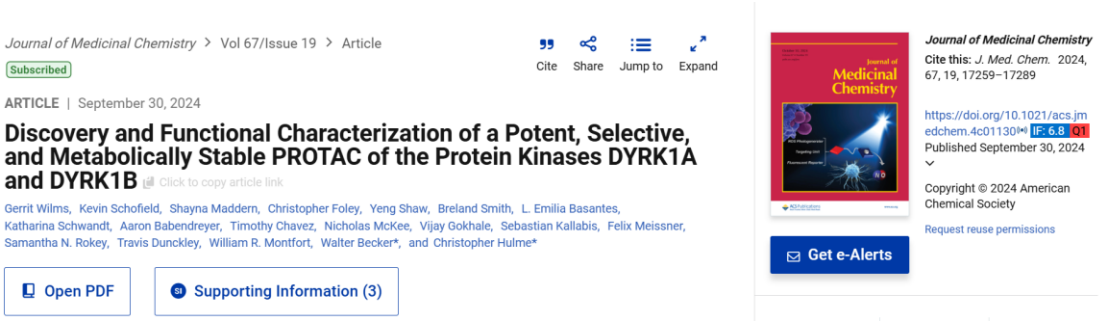


**Background:**

Bispecific tyrosine phosphorylation-regulated kinase 1A (DYRK1A) is a highly conserved protein kinase, widely expressed in human tissues, and is a major regulator of cell proliferation and differentiation, which is closely related to neurodegeneration, tumor progression, inflammation, diabetes, myocardial infarction, viral infections and other diseases. The catalytic domain of DYRK1B has 85% sequence homology with DYRK1A, but it is more limited

in cell expression type, which is regarded as a potential cancer drug target. The overactivity of DYRK1A and DYRK1B (collectively referred to as DYRK1) in disease has led to the development of DYRK1 inhibitors, which are mostly classical type 1 kinase inhibitors that interfere with enzyme activity by occupying ATP-binding sites and make it difficult to distinguish between DYRK1A and DYRK1B.

Molecular-induced targeted protein degradation is a promising approach in drug discovery and development, and PROTACs (proteolysis-targeting chimeras) act as heterobifunctional molecules to induce ubiquitination and degradation of target proteins by recruiting E3 ubiquitin ligases. However, DYRK1A is resistant to a variety of degraders. In addition to DYRK PROTACs, DYRK1A can also be degraded by CaNDY and DYR219 by other mechanisms, but this requires a long incubation and high drug concentrations, which somewhat limits the use of CaNDY and DYR219 as chemical probes.

In this study, DYRK1 PROTAC was developed for the first time by combining an ATP-competitive DYRK1 inhibitor with the E3 ligase ligand CRBN. Among them, compound DYR684 induces the effective degradation of DYRK1A and DYRK1B in a proteasome-dependent manner, and has stronger DYRK1 inhibitory activity than traditional kinase inhibitors.

## Results & Discussion

### Determination of target protein-binding ligands

DYR530 is a high-affinity DYRK1A inhibitor developed after structure-activity relationship studies on DYR219, which has better selectivity and pharmacokinetic properties than DYR219. The researchers identified the linker attachment site by resolving the eutectic structure of DYRK1A and DYR530. The binding of DYR530 to the ATP site is consistent with the type I kinase inhibitor profile. The 2-aminopyridine and imidazopyridine rings of DYR530 penetrate deep into the ATP binding pocket and form hydrogen bonds with Lys188, Glu203, Asp307 and Leu241 in the hinge region, 2-aminopyridine interacts with Val306 and Phe238 van der Waals, and imidazopyridine rings interact with Phe238, Leu294, Leu241, Met240 and Ala186 form van der Waals interactions. N-methylpiperazine has less contact with the protein and is oriented towards the solvent region, making it an ideal linker attachment site.

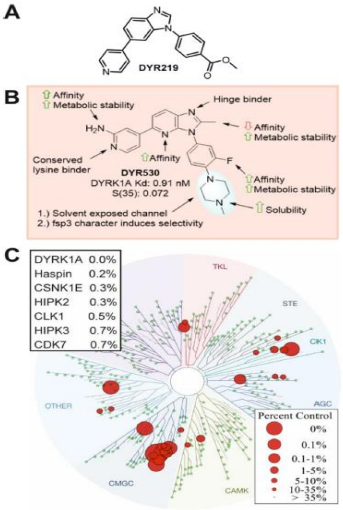


**Figure 1.** Precursor to and profile of the DYRK1 inhibitor DYR530. (A) Structure of the previously reported DYRK1 inhibitor DYR219. (B) Structure of DYR530 with structure activity and property relationships. The S(35) score is a measure of selectivity and is defined as the % of tested kinases that were measured to be <35% of control. (C) KinomeScan of DYR530 at 1 $\mu$M for 468 kinases. Kinases interacting with DYR530 are represented by red circles. The diameter of the circles indicates relative binding to the respective kinase. Targets scoring <1% are listed. Complete results are listed in the Supporting Information.

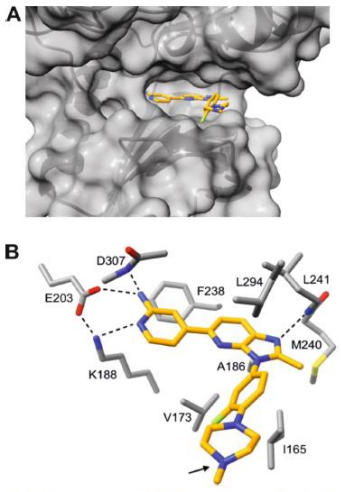


**Figure 2.** Crystal structure of DYRK1A in complex with DYR530 (PDB entry 8T2H). (A) Binding of DYR530 to the active site of DYRK1A. DYR530 is shown in orange, DYRK1A in gray. (B) Key interactions of DYR530 mapped in the ATP pocket. Backbone atoms of labeled residues are not shown except for D307 and L241, both involved in interactions. The linker attachment site is marked with an arrow. Complete crystallographic data is provided in the Supporting Information.

**Design and structural optimization of DYRK1 PROTAC**

DYR617-619, DYR625, and DYR622-624 were obtained by attaching PEG linkers of different lengths to the piperazine moiety of DYR530 and then to VHL ligand 1 or CRBN ligand pomalidomide, respectively. The degradation ability of these compounds to DYRK1A and DYRK1B was evaluated in HEK293 cells, and the results showed that CRBN-based PROTACs could significantly reduce the level of DYRK1A in cells, while VHL-targeting molecules could not effectively degrade DYRK1A. Extending the length of the linker of CRBN PROTAC can promote the degradation of DYRK1, for example, PROTAC with 4-PEG as linker (DYR624 - 60% *Dmax* DYRK1A) is better than PROTAC with 2-PEG as linker (DYR622 - 40% *Dmax* DYRK1A).

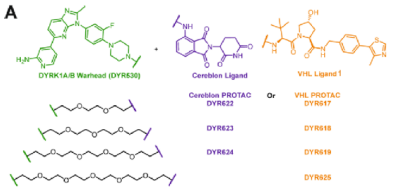


B

| ID | E3 ligase binder | $K_D$ (nM) (D1A/D1B) | $D_{0.3\mu M}$ (%) (D1A/D1B) |
|---|---|---|---|
| DYR617 | VHL | 3.4/5.5 | 11/0 |
| DYR618 | VHL | 2.2/6.9 | 5/2 |
| DYR619 | VHL | 1.3/3.6 | 0/0 |
| DYR625 | VHL | 1.4/6.6 | 0/0 |
| DYR622 | CRBN | 1.4/2.4 | 40/0 |
| DYR623 | CRBN | 1.4/3.5 | 52/25 |
| DYR624 | CRBN | 2.3/3.4 | 60/28 |

Figure 3. Development and characterization of DYRK1A/1B degraders. Chemical structures (A) and $K_D$ and degradation efficacies (B) of DYRK1A (D1A) and DYRK1B (D1B) degraders derived from DYR530. $K_D$ values were measured by competition binding assay ($K_d$ ELECT). Cellular degradation was determined in HEK293 cells overexpressing HiBiT-tagged DYRK1 constructs (HiBiT lytic assay, values represent % degradation after treatment with 0.3 $\mu$M of the compounds relative to vehicle-treated cells).

Next, the researchers proceeded to optimize the structure of the linker and CRBN ligand moieties. DYR665, DYR696 and DYR697 were obtained by coupling polyethylene glycolamine, piperazine, azidine and thalidomide at the three positions. DYR662, DYR666, DYR661 and DYR660 were obtained by introducing the CRBN E3 ligase regulator CC-220 (iberdomine). DYR667, DYR684 and DYR685 were obtained by introducing the high-affinity CRBN ligand 5-aminothiamine 100. The activity evaluation results showed that the degradation ability of DYRK1A was significantly improved for some compounds, and they also had a certain degradation effect on DYRK1B. Among them, DYR684 had the best activity, indicating that pyridine-piperidine may be an essential structure for activity.

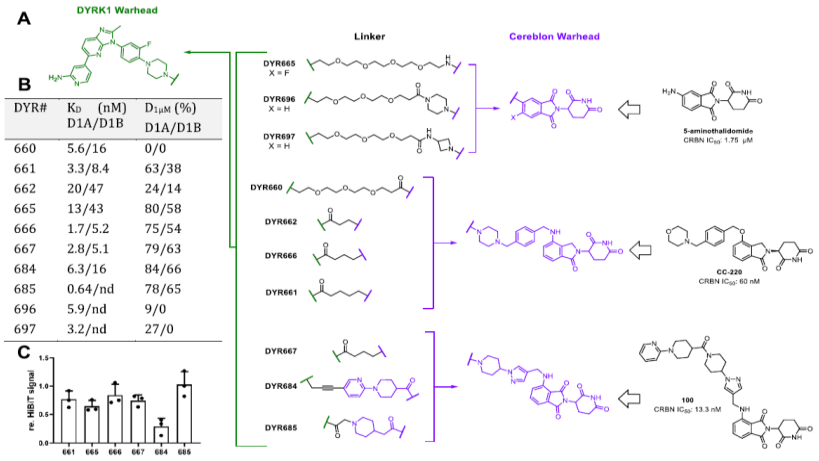


B

| DYR# | $K_D$ (nM) D1A/D1B | $D_{1\mu M}$ (%) D1A/D1B |
|---|---|---|
| 660 | 5.6/16 | 0/0 |
| 661 | 3.3/8.4 | 63/38 |
| 662 | 20/47 | 24/14 |
| 665 | 13/43 | 80/58 |
| 666 | 1.7/5.2 | 75/54 |
| 667 | 2.8/5.1 | 79/63 |
| 684 | 6.3/16 | 84/66 |
| 685 | 0.64/nd | 78/65 |
| 696 | 5.9/nd | 9/0 |
| 697 | 3.2/nd | 27/0 |




Figure 4. Development and characterization of DYRK1 degraders. Structures (A) and evaluation (B, C) of DYRK1A degraders derived from DYR530. $K_D$ values and degradation efficacies were determined as in Figure 3. In (B), cells were treated with 1 $\mu$M of compound, while in (C) selected compounds were evaluated at 300 nM (mean and SD, $n$ = 3). CRBN binding affinity for CC-220 was taken from ref 32. nd, not determined.

**Structural characteristics of DYR684**

The simulation results of DYRK1A/DYR684/CRBN ternary complex showed that DYR684 crossed the DYRK1A ATP pocket and the CRBN thalidomide binding site, forming multiple protein-protein interactions, salt bridge

interactions and hydrogen bond interactions, which were closely related to the efficacy and selectivity of DYR684. Analysis of kinome selectivity of DYR684 revealed that it hit fewer kinases than DYR530. This result is consistent with previous studies that significantly reduced the number of target kinases bound to type 1 kinase inhibitors by adding linkers and E3 recruiting ligand moieties.

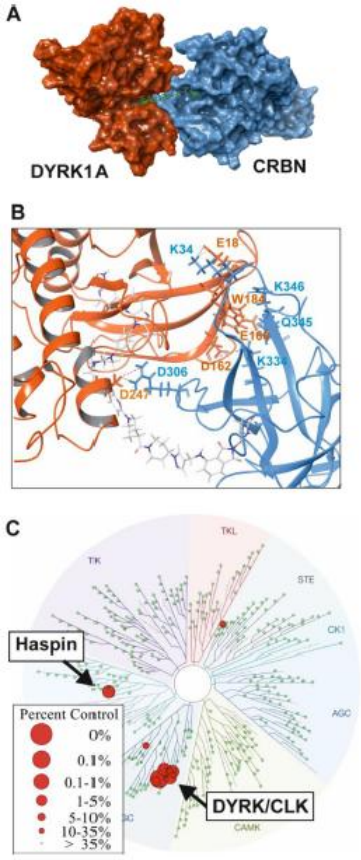


Figure 5. Characterization of DYR684. (A) Model of the ternary complex of DYR684 (green) bound to the catalytic domain of DYRK1A (red-orange) and the thalidomide-binding domain of CRBN (blue). (B) Ternary complex and protein−protein interactions (PPIs) observed between DYRK1A (red-orange) and CRBN (blue). Models were generated PRosettaC and figures were developed from Maestro. (C) KinomeScan of DYR684 at 1 μM. DYR684 targets 11 out of 468 kinases (S(35) score 0.024). Target kinases scoring <1% are labeled. Complete results are listed in the Supporting Information.

**Development of non-degradable analogues of DYR684**

DYR813 is obtained by methylation of the nitrogen atom on glutarimide. The DYRK1 degradation curve showed that DYR813 moderately reduced DYRK1A levels at higher concentrations, while DYR813 did not affect DYRK1A levels at lower concentrations (100 nM), indicating that the DYRK1A degradation activity of DYR684 was associated with CRBN recruitment.

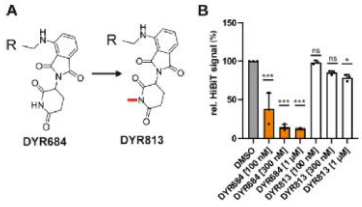


Figure 6. Validation of DYR813 as an inactive control compound. (A) *N*-methylation of DYR684 leads to DYR813. The methyl group prevents CRBN binding. (B) DYRK1A degradation assay. HEK293 cells expressing HiBiT-tagged DYRK1A were treated with the test compounds for 24 h before cellular DYRK1A levels were quantitated (HiBiT lytic assay). Results were normalized to the vehicle-treated control samples (means and SD, $n = 3$). Statistical differences to the control are indicated by asterisks (* $p < 0.05$, ** $p < 0.01$, *** $p < 0.001$).

**DYR684 concentration-dependent degradation of DYRK1**

Treatment of HEK293 cells with DYR684 for 24 h revealed that DYR684 reduced the levels of DYRK1A and DYRK1B in a concentration-dependent manner, with a DC50 value of 12.3 nM for DYRK1A and a maximum percent degradation of approximately 90% for DYRK1A and 50% for DYRK1B. None of the traditional type 1 inhibitors DYR530, L41, or CaNDY were effective in reducing DYRK1 levels. In addition, DYR684 does not alter the level of the adaptor protein DCAF7. The decrease in potency of DYR684 at high concentrations can be attributed to the "hook effect", which is typical of heterobifunctional ligands that rely on ternary complexes to form.

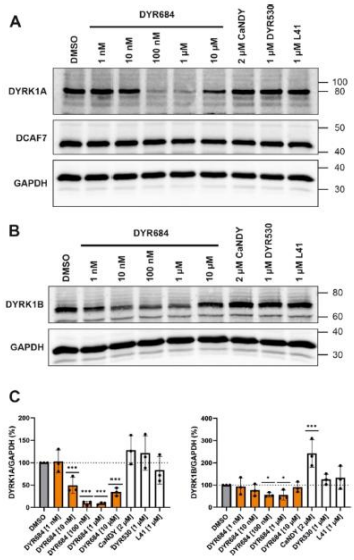


**Figure 7.** DYR684 reduces cellular DYRK1 levels. HEK293 cells were treated for 24 h with serial dilutions of DYR684 or control compounds (CaNDY, DYR530, L41). Total cellular lysates were analyzed by immunoblotting for levels of native DYRK1 (A, B). For quantitative evaluation (C), signals were normalized to loading controls (GAPDH). The graphs show means and SD ($n = 3$). Statistical differences to the control are indicated by asterisks (* $p < 0.05$, ** $p < 0.01$, *** $p < 0.001$).

**Time-dependent evaluation**

Treatment of HEK293 cells with 100 nM of DYR684 resulted in almost maximal degradation of DYRK1A and DYRK1B in HEK293 cells within 8 hours, followed by reappearance of DYRK1B, while the effects of DYR684 on DYRK1A lasted for at least 48 hours, but the restoration of DYRK1B levels was not associated with increased gene expression. Finally, the researchers assessed the duration of DYR684-mediated degradation after elution and found that DYRK1A levels did not recover within 48 hours of elution, suggesting that DYR684 has a sustained role in degrading DYRK1A under these conditions.

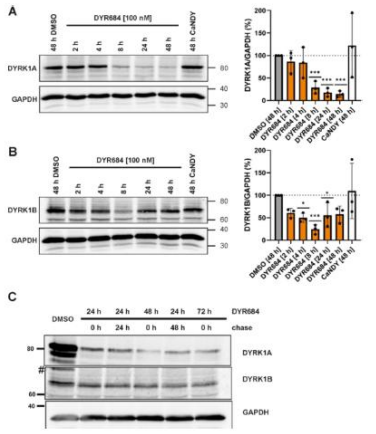


**Figure 8.** Time course of DYRK1 degradation by DYR684. HEK293 cells were treated with 100 nM DYR684, 2 $\mu$M CaNDY or vehicle (DMSO) before native DYRK1 levels were assessed by immunoblot analysis. (A, B) The left panels illustrate representative blots and the graphs show the quantitative evaluation (means and SD, $n$ = 3,). The two DYRK1B bands were evaluated together. Statistical differences from the control are indicated by asterisks (* $p < 0.05$, ** $p < 0.01$, *** $p < 0.001$). (C) HEK293 cells were treated with 100 nM DYR684 for the times indicated. DYR684 was reapplied with the daily medium change or was washed out (chase). The persisting DYRK1B band is due to the p65 splicing variant (see below). The blots are representative of 3 experiments. The hashtag marks the residual signal from the DYRK1A band that was detected before.

## The DYRK1B splice variant p65 is resistant to DYR684-induced degradation

In Figures 7 and 8, DYRK1B has dual bands representing p69 and p65, and the residual DYRK1B signal is mainly caused by the faster-migrating p65 variant, and further experiments confirm the selectivity reduction of the p69 variant. DYRK1B-p65 lacks 40 amino acids within the kinase domain and is a pseudokinase with no catalytic activity and potential resistance to PROTACs. Analysis of the HEK293 cell line with stable overexpression of HiBiT-tagged DYRK1B-p65 showed that treatment with 1 µM DYR684 resulted in a more significant reduction in DYRK1A abundance than DYRK1B-p69, while DYRK1B-p65 was completely resistant to degradation, possibly because PROTACs could not bind to the changed catalytic domain.

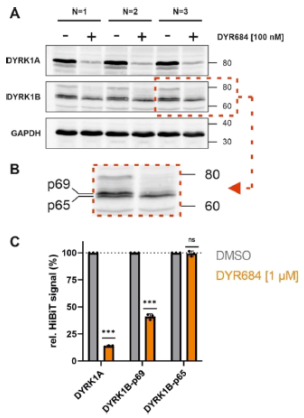


**Figure 9.** DYRK1B-p65 is resistant to DYR684-induced degradation. (A) Differential degradation of the native DYRK1B splicing variants p69 and p65. The Western blot illustrates the detection of DYRK1B in total cell lysates of HEK293 cells that were treated with DYR684 or vehicle for 24 h ($n$ = 3). (B) Cropped enlargement. (C) Degradation assay in HEK293 cells overexpressing HiBiT-tagged DYRK1A, DYRK1B-p65 or DYRK1B-p69. Cells were treated with 1 $\mu$M DYR684 or vehicle (DMSO) for 24 h. The results were normalized to the vehicle-treated control samples (means and SD, $n$ = 3). Statistical differences from the control are indicated by asterisks (* $p < 0.05$, ** $p < 0.01$, *** $p < 0.001$).

## DYR684 induces DYRK1 proteasome degradation via CRBN-mediated ubiquitination

Pretreatment of HEK293 cells with excess L41 or lenalidomide was found to prevent endogenous DYRK1A/B degradation, suggesting that CRBN binding is necessary for the degradation of DYR684. Pretreatment with a NEDD8 activating enzyme (NAE) inhibitor MLN4924 also attenuates the degradation of DYRK1A/B, suggesting that the degradation of DYR684 involves the ubiquitin ligase CRL. Treatment with p97 unfolding enzyme inhibitor inhibited

the degradation of DYRK1A/B, suggesting that p97 unfolding is essential for protein kinase degradation. Treatment with the proteasome inhibitor bortezomib confirmed that the degradation of DYRK1A/B is dependent on proteasome activity. Overexpression experiments verified the binding of ubiquitin to DYRK1A. In conclusion, the above results suggest that DYR684 recruits the E3 ligase ligand CRBN to induce DYRK1A/B ubiquitination, followed by p97-mediated unfolding and proteasomal degradation.

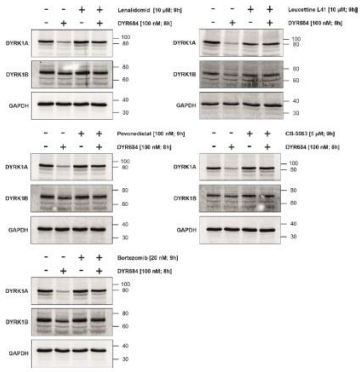


**Figure 10.** Mechanism of DYR684-induced DYRK1A/B degradation. HEK293 cells were pretreated with lenalidomide, L41, pevonedistat, CB-5083, bortezomib, or vehicle (DMSO) before application of DYR684. Each image is representative of 3 experiments.

The sequential steps of degradation collectively influence the PROTAC-induced target degradation kinetics. To characterize the degradation of DYRK1 in real time, HEK293 cells stably expressing GFP-DYRK1A or GFP-DYRK1B fusion proteins were treated with DYR684 or the non-degradable analogue DYR813 for 6 hours to monitor GFP fluorescence. The results showed that GFP-DYRK1A was rapidly and efficiently degraded at an initial degradation rate of about 0.74 $h^{-1}$ (*t1/2* = 57 min), and GFP fluorescence was reduced by up to 98%. GFP-DYRK1B was degraded at a rate of 1.16 $h^{-1}$ (*t1/2* = 36 min) and reached a plateau at 86% degradation. The rapid degradation of overexpressed DYRK1A and DYRK1B by 1 µM DYR684 suggests that when endogenous DYRK1 is degraded by 100 nM of DYR684, the individual mechanistic steps involved in proteasome degradation are not saturated, so this treatment is unlikely to negatively affect cellular protein quality control systems.

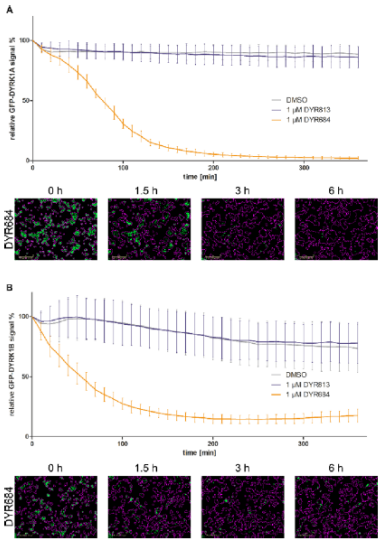


**Figure 11.** Kinetics of DYR684-induced degradation of overexpressed GFP-DYRK1A/B. Loss of GFP fluorescence was monitored by automated live cell fluorescence microscopy of HEK293 cells with stably integrated expression modules for GFP-DYRK1A (A) or GFP-DYRK1B (B). GFP fluorescence (green) was measured by using the green object mask, and total surface area coverage by the cells (purple) was determined by phase contrast microscopy. The graphs show the fluorescence intensities over time after treatment with DYR684, DYR813 or solvent alone (means and SD, $n = 3$). See Figure S5 for microscopic images of DMSO- or DYR813-treated cells.

**Degradation of DYRK1A in cancer cell lines**

DYRK1A and DYRK1B are potential drug targets for cancer therapy. Different human cancer cell lines were treated with DYR684 for 8 hours, and the results showed that DYR684 had a cell line-specific effect, and DYRK1A was completely or substantially degraded in SH-SY5Y neuroblastoma and A549 lung adenocarcinoma cells. In PANC-1 pancreatic cancer cells, DYRK1A is partially degraded; HeLa cervical cancer cells and OVCAR3 ovarian cancer cells are resistant to DYR684. Sustained depletion of DYRK1A and DYRK1B is observed when SH-SY5Y and A549 cells are treated with DYR684 for 24 h.

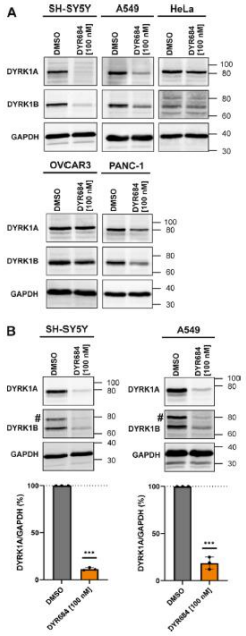


**Figure 12.** Effect of DYR684 in cancer cell lines. (A) Cells were treated with 100 nM DYR684 for 8 h. (B) Cells were treated for 24 h, and effects were quantitated (means and SD, $n = 3$). Statistical differences to the control are indicated by asterisks (* $p < 0.05$, ** $p < 0.01$, *** $p < 0.001$). The hashtag marks the residual signal from the DYRK1A band that was detected before.

**Effect of DYR684 on DYRK1 activity in cells**

To evaluate the effect of DYR684 on DYRK1A/B downstream targets, the researchers evaluated the phosphorylation of SF3B1. DYR684 at 10 nM inhibits near-maximumal phosphorylation of SF3B1, and the decrease in SF3B1 phosphorylation may be due to direct inhibition of DYRK1 activity or due to PROTAC-induced degradation. By comparing the effect of DYR684 with the non-degradable control DYR813, it was found that DYR813 partially inhibited the phosphorylation of SF3B1, indicating that it could bind DYRK1 and block the ATP binding site, and also showed that DYRK1 was not completely occupied at a concentration of 100 nM, indicating that maximum target binding is not necessary for high efficiency for drugs that act through an "event-driven" mechanism.

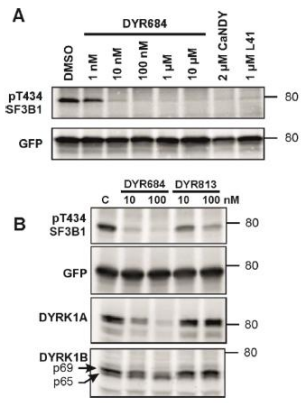


**Figure 13.** Effect of DYR684 on DYRK1 downstream signaling. (A) HEK293 cells transiently expressing GFP-SF3B1 were treated with variable concentrations of DYR684 for 48 h before the phosphorylation of SF3B1 on Thr434 was detected by immunoblot analysis. CaNDY and L41 served as positive controls. The blot is representative of $n = 3$ experiments. (B) Cells were treated with DMSO, DYR684 or DYR813 for 24 h. Arrows point to the DYRK1B splicing variants (p65 and p69).

## Effect of DYR684 on the proteome

To explore the degradation selectivity of DYR684 at the proteomic level, the researchers performed an unbiased quantitative global proteomic analysis. More than 6500 proteins were quantified after 24 hours of treatment with 100 nM of DYR684 or solvent in HEK293 or SH-SY5Y cells, and DYRK1A was found to be the only protein kinase significantly degraded. DYRK1B was not detected in HEK293 cells. Consistent with the Western blot results, DCAF7 levels were not affected by DYR684. A very small number of proteins show significant changes after treatment.

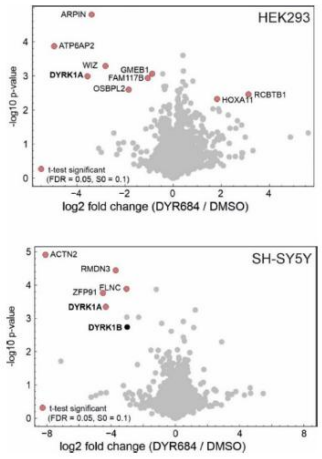


**Figure 14.** Global proteomic changes induced by DYR684. The volcano plots show relative abundance of proteins in HEK293 cells and SH-SY5Y cells that were treated for 24 h with DYR684 (100 nM) or vehicle against significance levels (−log10 (p-value) ($n = 4$ for HEK293, $n = 3$ for SH-SY5Y). Significantly downregulated proteins are found in the upper left quadrant of the plots (red dots). For the list of proteins with significant changes see Table S1 in the Supporting Information.

## Cytotoxic effects of DYR684 in SH-SY5Y neuroblastoma cells

Since DYRK1A and DYRK1B are drug targets for cancer therapy, the researchers investigated the role of DYR684 in SH-SY5Y neuroblastoma cells. Treatment of cells with 2 µM cisplatin, 100 nM DYR684, or both resulted in moderate cytotoxicity, and macroscopic observation showed a significant increase in cell death, suggesting that DYR684 reduced the viability of neuroblastoma cells and could be used in combination with cisplatin.

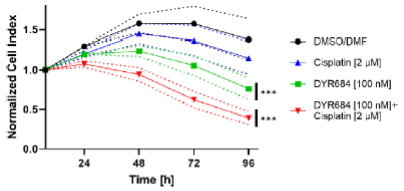


**Figure 15.** Cytotoxicity of DYR684 and cisplatin on SH-SY5Y cells was monitored by real time electrical impedance measurements. The normalized cell index is proportional to the impedance, which reflects cell number and cell attachment (means and SEM, $n = 4$). For statistical analysis, area under the curve (AUC) values from 7–96 h after treatment were calculated. Significant differences to the control are indicated by asterisks (*** $p < 0.001$).

## Physicochemical and pharmacokinetic properties of DYR684

The solubility of DYR684 in biocorrelation buffers is low, but well above the DC50 value. DYR684 has good stability in liver microsomes and whole blood. DYR684 is highly protein-binding, and PAMPA data suggest that it has difficulty crossing the blood-brain barrier. Kinetic analysis showed that DYR684 had a long residence time and slow dissociation. The pharmacokinetic parameters in mice showed that DYR684 was rapidly absorbed after intraperitoneal injection, and the plasma concentration could be maintained above the DC50 value for a certain period of time, which could achieve the maximum degradation of DYRK1. The high plasma protein binding of DYR684 results in a relatively low clearance.

In vivo metabolite identification of DYR684 has not been performed. It is speculated that pomalidomide structure may be a factor contributing to its plasma instability, and that changing phthalimide-glutarimide to phenyglutarimide can increase plasma stability. Xenosite software predicts that N-dealkylation and glucuronidation may be the main metabolic pathways of DYR684.

**Table 1. *In Vitro* Physicochemical and Pharmacokinetic Properties of DYR684**

| | |
|---|---|
| **Physicochemical properties** | |
| molecular weight | 1064.20 |
| hydrogen bond acceptor | 19 |
| hydrogen bond donor | 3 |
| total polar surface area | 260.98 |
| no. of rotatable bonds | 9 |
| solubilities in PBS/FaSSIF/FeSSIF[a] | <0.0087/0.16/2.03 $\mu$M |
| **Pharmacokinetic properties** | |
| $T_{1/2}$ in mouse plasma | 6.97 h |
| $T_{1/2}$ in mouse/rat/human liver microsomes | 7.38/1.64/2.28 h |
| $CL_{int}$ in mouse/rat/human liver microsomes | 3.1/14.0/10.1 mL/min/kg |
| $T_{1/2}$ in mouse blood | 15.15 h |
| PAMPA[b] ($P_e$) | <0.005 × 10−6 cm/s |
| % plasma protein bound | >99.38 |
| Caco-2 permeability A-B | <0.270 × $10^{-6}$ cm/s |
| Caco-2 permeability B-A | <0.243 × $10^{-6}$ cm/s |
| **Kinetic profiling of target binding** | |
| $K_d$ for DYRK1A/B | 6.3/16 nM |
| DYRK1A residence time | 23 min |
| $k_{on}$ | 1.83 × $10^5$ $M^{-1}$ $s^{-1}$ |
| $k_{off}$ | 7.25 × $10^{-4}$ $M^{-1}$ $s^{-1}$ |

[a]PBS, phosphate buffered saline, FaSSIF/FeSSIF, Fasted/Fed State Simulated Intestinal Fluid. [b]PAMPA, parallel artificial membrane permeability assay.

**Table 2. *In Vivo* Pharmacokinetic Parameters of DYR684 following a Single Dose of DYR684 (Averaged Over Three Mice)**

| | *IV*[a] (1 mg/kg) | *IP*[b] (*10* mg/kg) | *PO*[c] (*10* mg/kg) |
|---|---|---|---|
| CL (L/h/kg) | 7.1 | | |
| $Vd_{ss}$ (L/kg) | 0.614 | | |
| Tmax (h) | | 0.25 | 0.5 |
| Cmax (ng/mL) | | 8127 | 18.5 |
| $T_{1/2}$ (h) | 3.33 | 4.75 | 2.11 |
| $AUC_{last}$ (h·ng/mL) | 2456 | 26,303 | 56 |
| $AUC_{inf}$ (h·ng/mL) | 2472 | 27,064 | 64 |
| MRT (h) | 1.4 | 5.77 | 2.51 |
| F (%) | | 109 | 0.25 |

[a]IV, intravenous. [b]IP, intraperitoneal. [c]PO, peroral; CL, clearance; $Vd_{ss}$, volume of distribution; $T_{max}$, the time to reach the maximum plasma concentration; $C_{max}$, the maximum plasma concentration reached; AUC area under the curve from time of dosing to the time of last quantifiable concentration (AUClast) or extrapolated to infinity (AUCinf), MRT, mean resident time; F, bioavailability

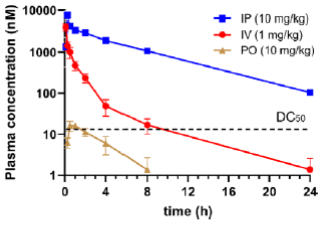


**Figure 16.** Mean plasma concentration–time profiles of DYR684 after single intraperitoneal (IP), intravenous (IV) and peroral (PO) administration. Data are expressed as mean ± SD ($n = 3$). The dotted line marks the $DC_{50}$ for DYRK1A in HEK293 cells. Error bars of the IP measurements are too small to be seen.

**Summary**

In this study, DYR684, a CRBN-recruiting degrader, was developed based on DYRK1 inhibitor DYR530, which confirmed for the first time that DYRK kinase can be degraded by PROTACs. DYR684 meets key criteria for chemical probes in terms of physicochemical and pharmacokinetic properties, potency, target selectivity, mechanism validation, and availability of non-degradable control compounds. Compared with traditional type 1 inhibitors, DYR684 can consistently and effectively reduce DYRK1A signaling and has different effects on different splice variants of DYRK1B. Further optimizations of DYR684 are ongoing to improve pharmacokinetic properties and selectivity to advance the clinical translation of DYRK1 degraders.

Reference: 10.1021/acs.jmedchem.4c01130

1. Combined with drug design ideas, Pharmacodia CyberSAR excavates the active structure reported in the literature and patents, and uses CyberSAR to facilitate and quickly obtain the target structure of interest of R&D personnel for developing ideas, and the following is an example of DYRK1A, one of the targets in this paper

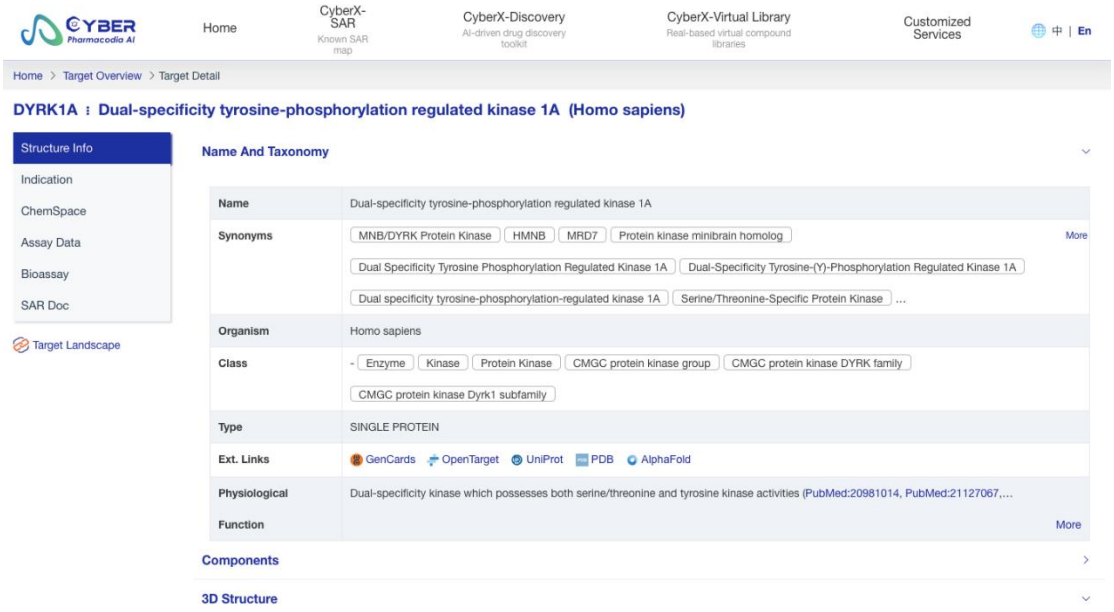


2. Select the "Cluster Structure View" tab under the "Chemical Space" option tab in the target interface, and the molecules with experimental test activity related to the target included in the CyberSAR platform can be displayed in the form of "parent nuclear structure clustering". Among them, the "highlighted in green" refers to the active molecular structure of IC50 < 1000 nM in the in vitro enzyme and cell activity test experiments reported in the literature, the specific experiments, experimental results and experimental sources.

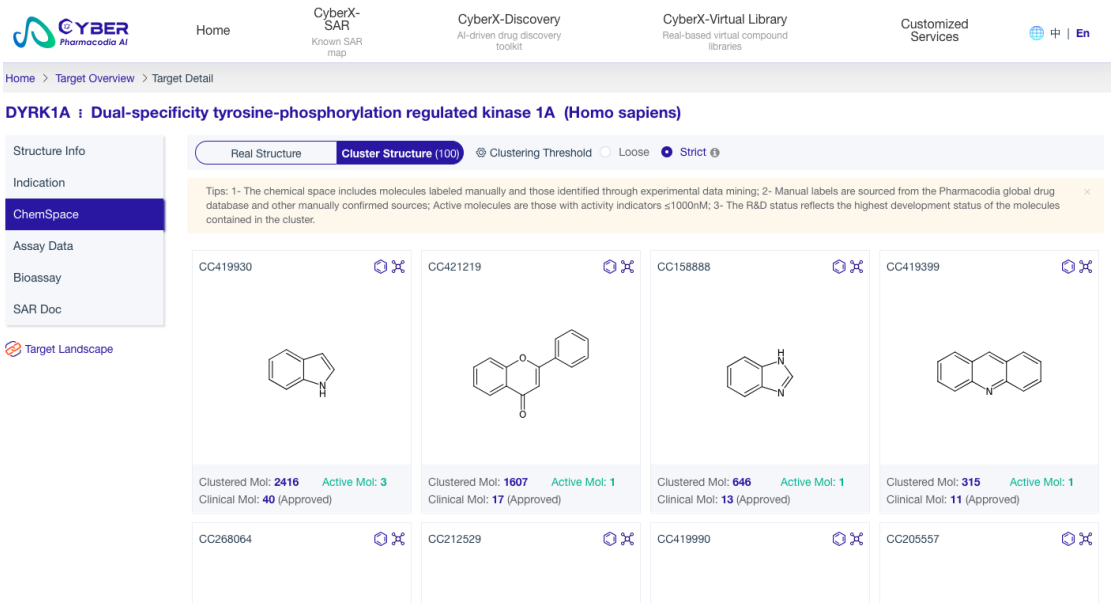


3. Select the "Real Structure View" tab under the "Chemical Space" option tab in the target interface, and the molecules with target-related experimental test activity included in the CyberSAR platform can be displayed in the form of "R&D stage timeline". Among them, the green color highlights the potential Hit.

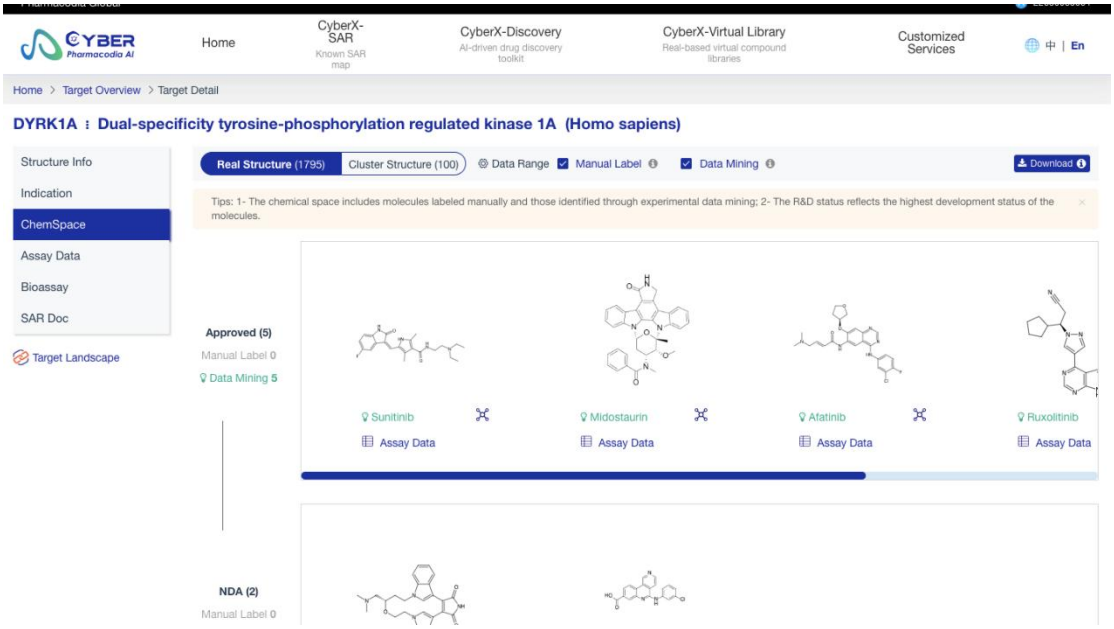


4. Select the "Indications" option label in the target interface, and you can visually and intuitively analyze all kinds of big data collected.

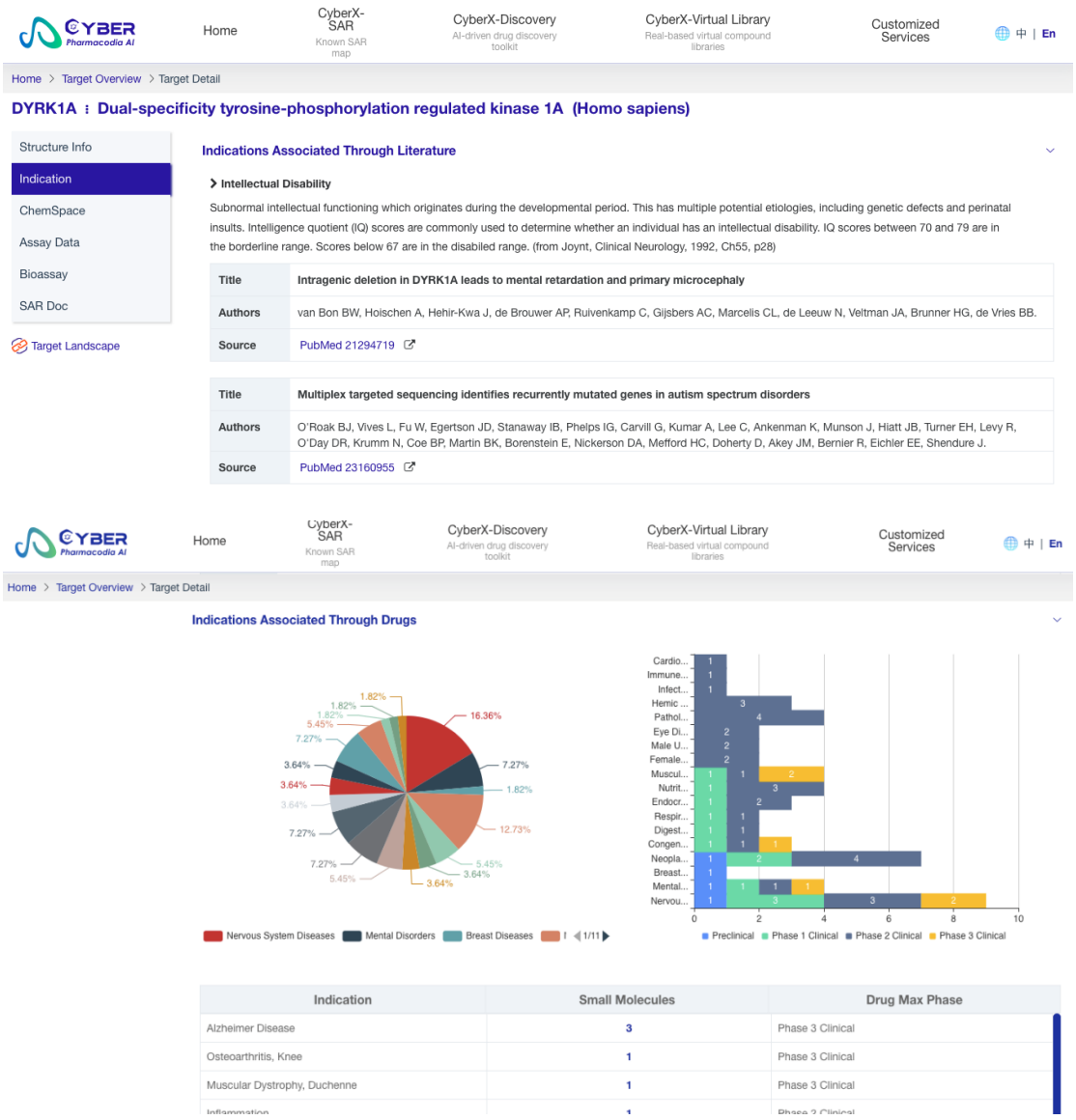





| Indication | Small Molecules | Drug Max Phase |
|---|---|---|
| Alzheimer Disease | 3 | Phase 3 Clinical |
| Osteoarthritis, Knee | 1 | Phase 3 Clinical |
| Muscular Dystrophy, Duchenne | 1 | Phase 3 Clinical |

*To Explore Cyber-AIDD further Login on your computer using the below Link*

**https://cyber.pharmacodia.com/#/homePage**

If you need further assistance contact us,


## For a free trial, Contact us on

**Anil Ranadev**
+91 9742627845
anil_ranadev@saspinjara.com

**Aravind P**
+91 9619076286
aravind.p@saspinjara.com

**Sachin Marihal**
+91 9538033363
sachin.marihal@saspinjara.com

**Chetan S**
+91 7022031061
chetans@saspinjara.com